State Estimation of a Thermal Model of Air-cooled Synchronous Generator

Madhusudhan Pandey, Thomas Øyvang, Bernt Lie

University of South-Eastern Norway, Porsgrunn, Norway, Bernt.Lie@usn.no

Abstract

In this paper, we extend a previous study on a totally enclosed thermal model of a synchronous generator, with temperature state estimation using experimental data. The extension includes a new formulation of the system model, with four different model variations with and without temperature dependence in the metal, air, and water heat capacities and the copper resistances, where temperature variation in water and/or air requires a non-standard heat exchanger model. In the former study, the Unscented Kalman Filter (UKF) was used for state estimation. Here, we include both the UKF as well as the Ensemble Kalman Filter (EnKF) in the comparison. UKF and EnKF are compared based on estimation accuracy and computational speed. Results show that EnKF exhibits lower RMSE for the innovation process and thus is more accurate than the UKF even with a "minimum" of 50 particles, but the UKF with 6 sigma points (3 states) is faster. It is too early to conclude which of 4 models is more accurate, as they need to be tuned individually wrt. parameter fitting.

Keywords: Air-cooled synchronous generator, dynamic model, state estimation, Unscented Kalman filter, Ensemble Kalman filter

1 Introduction

1.1 Background

Due to the increase in intermittent renewable energy resources, hydropower plants will become a key component to provide higher operational flexibility in the future power system. In European hydropower generation, the synchronous generator power factor is restricted to the range $[0.85, 0.95]$, (ENTSO-E, 2016); for Norway, the power factor should be less than 0.86, (Statnett, 2012).

The power factor is the ratio of active power to apparent (complex) power. A small power factor implies a reduced active power production compared to a higher power factor. High production of active power is desired by the plant owners, but an increased power factor may cause problems due to the thermal design limitation of the machine. An important question is: would it be acceptable to relax on the constraint on the power factor for a limited time period in order to take out unexploited power in critical situations? To allow for such a relaxation in the power factor, it is important to have a measure of the temperature evolution, and how this influences the lifetime of the generator.

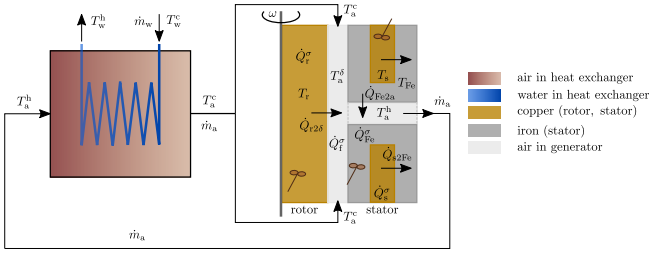

Figure 1. Thermal model of air-cooled synchronous generator, from (Lie, 2018).

In this paper, we consider how to obtain information about the temperature evolution.

A thermal model of a totally enclosed air-cooled hydro generator was developed in (Øyvang, 2018), using a closed-loop, water cooled heat exchanger for cooling heated air from the outlet of generator, and applied to a case study of a vertically mounted 103 MVA air-cooled hydro generator at Åbjøra, Norway. A similar model with more general structure and more efficient heat exchanger description was developed in (Lie, 2018).

It is of interest to extend the description in (Lie, 2018) with temperature dependent heat capacities (metals, air) and temperature dependent copper resistances. Furthermore, it is of interest to carry out a more extensive study on state estimation compared to (Øyvang, 2018), using several variations of the Unscented Kalman Filter (UKF) as well as introducing the Ensemble Kalman Filter (EnKF).

1.2 Organization of paper

The paper is organized as follows. The mathematical model is presented in Section 2. State estimation algorithms UKF and EnKF are presented in Section 3. Results are presented and discussed in Section 4. Finally, conclusions are drawn in Section 5, together with possible future work.

2 Mathematical model

Figure 1 shows the thermal operation of an air-cooled synchronous generator.

The cold air out of the heat exchanger is blown by a fan into the rotor/stator air gap. The air is heated by heat flow from rotor, air gap windage, and bearing friction. Next, air is forced into ducts through the stator iron core where it gets heated by heat flow from the iron. At the outlet

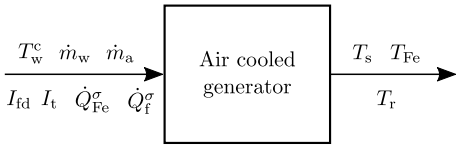

Figure 2. Functional diagram for air-cooled synchronous generator, from (Lie, 2018).

from the stator ducts, the heated air is collected and passed through a counter-current heat exchanger. The heated air is cooled down through the heat exchanger using continuous cold water circulation, before it is re-injected into the air gap in a continuous, closed loop process.

The water mass flow rate through the heat exchanger is $\dot{m}_w$, and it enters at temperature T_w^c and leaves the heat exchanger at temperature T_w^h. The air mass flow rate is $\dot{m}_a$ with temperature T_a^h at stator outlet and heat exchanger entry; through the heat exchanger, the air is cooled down to temperature T_a^c. The metal volumes are assumed to be homogeneous in temperature, with rotor copper at temperature T_r, stator copper at temperature T_s, and stator iron at temperature T_{Fe}. Rotor copper is heated by heat rate $\dot{Q}_r^{\sigma}$ due to resistive electric loss from the field current I_f. Similarly, the stator copper is heated by heat rate $\dot{Q}_s^{\sigma}$ due to stator terminal current I_t. The stator iron is heated by heat rate $\dot{Q}_{Fe}^{\sigma}$ due to eddy current losses and hysteresis losses, (Hargreaves et al., 2011). The air gap between rotor and stator is heated at heat rate $\dot{Q}_f^{\sigma}$ due to bearing and windage losses, (Øyvang, 2018). In addition, heat conduction/convection between the various volumes take place. It is of interest to consider how the inputs $\dot{m}_w$, $\dot{m}_a$, T_w^c, $\dot{Q}_{Fe}^{\sigma}$, $\dot{Q}_f^{\sigma}$, I_t and I_f influence the temperatures in the generator metals, T_r, T_s, and T_{Fe}. A functional diagram for the air-cooled synchronous generator is shown in Figure 2 relating inputs and outputs.

The mathematical model governing generator metal temperatures is taken from (Lie, 2018),

$$m_r \hat{c}_{p,Cu} \frac{dT_r}{dt} = 1.1 R_r I_f^2 - \mathscr{U} A_{r2\delta} \left(T_r - T_a^{\delta} \right) \quad (1)$$

$$m_s \hat{c}_{p,Cu} \frac{dT_s}{dt} = 3 R_s I_t^2 - \mathscr{U} A_{s2Fe} \left(T_s - T_{Fe} \right) \quad (2)$$

$$m_{Fe} \hat{c}_{p,Fe} \frac{dT_{Fe}}{dt} = \mathscr{U} A_{s2Fe} \left(T_s - T_{Fe} \right) - \mathscr{U} A_{Fe2a} \left(T_{Fe} - T_a^h \right) + \dot{Q}_{Fe}^{\sigma}. \quad (3)$$

Here, m_r, m_s, and m_{Fe} are the masses of the respective metal volumes. $\hat{c}_{p,Cu}$ and $\hat{c}_{p,Fe}$ are specific heat capacities of copper and iron, respectively. R_r and R_s are resistances of copper in the rotor and stator, respectively, $\mathscr{U} A_{r2\delta}$, $\mathscr{U} A_{s2Fe}$, and $\mathscr{U} A_{Fe2a}$ are heat transfer factors between rotor metal and rotor-stator air-gap, stator copper and stator iron, and stator iron and stator duct air gaps, respectively. T_a^{δ} and T_a^h are air temperatures in the rotor-stator air-gap and in the stator duct, respectively.

Similarly, for air inside the generator,

$$0 = \dot{m}_a \hat{c}_{p,a} \left(T_a^c - T_a^{\delta} \right) + \mathscr{U} A_{r2\delta} \left(T_r - T_a^{\delta} \right) + \dot{Q}_f^{\sigma} \quad (4)$$

$$0 = \dot{m}_a \hat{c}_{p,a} \left(T_a^{\delta} - T_a^h \right) + \mathscr{U} A_{Fe2a} \left(T_{Fe} - T_a^h \right). \quad (5)$$

Here, $\hat{c}_{p,a}$ is the specific heat capacity of air.

For the heat exchanger, we introduce *Stanton numbers* N_{St}^w and N_{St}^a,

$$N_{St}^w = \frac{\mathscr{U} A_x}{\hat{c}_{p,w} \dot{m}_w} \quad (6)$$

$$N_{St}^a = \frac{\mathscr{U} A_x}{\hat{c}_{p,a} \dot{m}_a} \quad (7)$$

$$N_{St}^{\Delta} = N_{St}^w - N_{St}^a. \quad (8)$$

Here, $\hat{c}_{p,w}$ is the specific heat capacity of water, and $\mathscr{U} A_x$ is the heat transfer factor between water and air in the heat exchanger. Provided that the Stanton numbers are constant and independent of (i) position, and (ii) temperatures, the counter-current heat exchanger model is

$$\left(N_{St}^w - N_{St}^a \exp\left(-N_{St}^{\Delta} \right) \right) T_a^c = N_{St}^{\Delta} T_a^h + N_{St}^a \left(1 - \exp\left(-N_{St}^{\Delta} \right) \right) T_w^c. \quad (9)$$

The heat exchanger model in 9 is the result of analytically solving a linear two point boundary value problem.

This model can be extended in several directions, by (a) introducing temperature dependence in the specific heat capacities $\hat{c}_{p,j}$, (b) introducing temperature dependence in the copper resistances R_r and R_s, and (c) in principle also in the heat transfer factors $\mathscr{U} A_j$. The only substantial change in the model is that if any of the Stanton numbers become temperature dependent, this will invalidate 9, and the involved two point boundary value problem must be solved numerically instead of analytically. Here, we assume constant Stanton numbers, even when the specific heat capacity of air is allowed to vary in 4–5.

To this end, four different models will be considered here:

- Model 1: constant values, $\hat{c}_p$, R
- Model 2: constant specific heat capacity, temperature dependent resistance, $\hat{c}_p$, $R(T)$
- Model 3: temperature dependent specific heat capacity, constant resistance, $\hat{c}_p(T)$, R
- Model 4: temperature dependence specific heat capacity and resistance, $\hat{c}_p(T)$, $R(T)$.

To simplify the discussion and avoid invalidating the heat exchanger model in 9, we will assume that specific heat capacity of air is constant in the heat exchanger but varies with temperature in the air gap/air duct, while we will introduce temperature dependence in copper and iron. To this end, for $\hat{c}_{p,j}(T)$, $j \in \{\mathrm{a,Cu,Fe}\}$, we will use a linear approximation given as,[1]

$$\hat{c}_{p,j}(T) = \frac{\mathscr{R}}{M_j}(a_j + b_j T), \tag{10}$$

where $\mathscr{R}$ is *universal gas constant* and M_j is the molecular mass. For the copper resistance,

$$R_j(T_j) = R_j^{\circ}(1 + \alpha_{\mathrm{Cu}}(T_j - T_{\mathrm{Cu}}^{\circ})), \quad j \in \{\mathrm{r,s}\} \tag{11}$$

where α_{Cu} is temperature coefficient of resistance for copper.

The parameters for the model of (Øyvang, 2018) are given in Table 1.

Operating conditions for the model are given in Table 2.

2.1 Overview of experimental data

A *heat-run test* of the synchronous hydro generator machine was performed for 600 min, (Øyvang, 2018). Table 3 lists measured quantities in the test.

Measurements were logged every minute for a supplied field current (I_{f}) from cold-start. The cold-run lasted 53 min, where the terminal voltage was built-up by residual flux in rotor windings. After the cold-run period, the supplied field current was increased leading to an increase in the measured stator copper and iron temperatures. The experimental results are displayed in Figure 3.

3 State Estimation

Notation used in the state estimation algorithms are given in Table 4.

A relatively general nonlinear system model can be represented as

$$x_{k+1} = f(x_k, u_k) + w_k \tag{12}$$

$$y_k = h(x_k) + v_k \tag{13}$$

with $w_k \sim \mathcal{N}(\bar{w}_k, \mathscr{W}_k)$ and $v_k \sim \mathcal{N}(\bar{v}_k, \mathscr{V}_k)$.

For our model, the state is $x = \begin{pmatrix} T_{\mathrm{r}} & T_{\mathrm{s}} & T_{\mathrm{Fe}} \end{pmatrix}$, while the measurements are $y = \begin{pmatrix} T_{\mathrm{s}} & T_{\mathrm{Fe}} \end{pmatrix}$. We wish to combine the measurements (y) with the state space model to estimate the unmeasured rotor copper temperature T_{r} and air gap temperature T_{a}^{δ}. To do that, we use two different Kalman Filter algorithms: the Unscented Kalman Filter (UKF) is presented in (Simon, 2006), while the Ensemble Kalman Filter (EnKF) is succinctly described in (Brastein et al., 2019). A summary of the UKF and EnKF algorithms are given in Tables 5 and 6, respectively.

[1] We will be considering linear approximation for temperature dependent specific heat capacity. The 7-coefficients, often called as NASA Lewis coefficients, power series form is given in (McBride et al., 2002; Zehe et al., 2002) which is converted to linear approximation for simplifying mathematical models.

Table 1. Parameters for air-cooled synchronous generator model. For the NASA Lewis coefficients, see 10.

Quantity	Symbol	Value
Atmospheric pressure	p_{a}	$1.01 \cdot 10^5\,\mathrm{N/m^2}$
Specific heat capacity, air	$\hat{c}_{p,\mathrm{a}}$	$1.15\,\mathrm{kJ/kg/K}$
Specific heat capacity, water	$\hat{c}_{p,\mathrm{w}}$	$4.2\,\mathrm{kJ/kg/K}$
Specific heat capacity, copper	$\hat{c}_{p,\mathrm{Cu}}$	$385\,\mathrm{J/kg/K}$
Specific heat capacity, iron	$\hat{c}_{p,\mathrm{Fe}}$	$465\,\mathrm{J/kg/K}$
Universal gas constant	$\mathscr{R}$	$8.314\,\mathrm{J/K/mol}$
Molar mass, air	M_{a}	$28.97\,\mathrm{g/mol}$
Molar mass, water	M_{w}	$18.01\,\mathrm{g/mol}$
Molar mass, copper	M_{Cu}	$63.54\,\mathrm{g/mol}$
Molar mass, iron	M_{Fe}	$55.84\,\mathrm{g/mol}$
NASA Lewis coefficient-linear approx., air	a_{a}, b_{a}	$3.28,\ 6.72 \cdot 10^{-4}$
NASA Lewis coefficient-linear approx., copper	a_{Cu}, b_{Cu}	$2.56,\ 1.2 \cdot 10^{-3}$
NASA Lewis coefficient-linear approx., iron	a_{Fe}, b_{Fe}	$0.19,\ 6.76 \cdot 10^{-3}$
Copper mass, rotor	m_{r}	$9260\,\mathrm{kg}$
Copper mass, stator	m_{s}	$6827\,\mathrm{kg}$
Iron mass, stator	m_{Fe}	$71.2 \cdot 10^3\,\mathrm{kg}$
Heat transfer, rotor to air gap	$\mathscr{U}A_{\mathrm{r2}\delta}$	$2.7\,\mathrm{kW/K}$
Heat transfer, stator copper to iron	$\mathscr{U}A_{\mathrm{s2Fe}}$	$20\,\mathrm{kW/K}$
Heat transfer, stator iron to air	$\mathscr{U}A_{\mathrm{Fe2a}}$	$14.3\,\mathrm{kW/K}$
Heat transfer, solid to air	$h_{\mathrm{a}}A_{\mathrm{x}}$	$55.6\,\mathrm{kW/K}$
Heat transfer, solid to water	$h_{\mathrm{w}}A_{\mathrm{x}}$	$222\,\mathrm{kW/K}$
Heat transfer, air to water	$\mathscr{U}A_{\mathrm{x}}$	$1/\left(\frac{1}{h_{\mathrm{a}}A_{\mathrm{x}}} + \frac{1}{h_{\mathrm{w}}A_{\mathrm{x}}}\right)$
Reference temperature air	T_{a}°	$25\,^{\circ}\mathrm{C}$
Rotor copper ohmic resistance, $T_{\mathrm{r}}^{\circ} = 15.7\,^{\circ}\mathrm{C}$	R_{r}°	$0.127\,\Omega$
Stator copper ohmic resistance, $T_{\mathrm{s}}^{\circ} = 20\,^{\circ}\mathrm{C}$	R_{s}°	$1.95\,\mathrm{m}\Omega$
Resistance nominal temperature	T_{Cu}°	$25\,^{\circ}\mathrm{C}$
Resistance temperature coeff.	α_{Cu}	$4.04 \cdot 10^{-3}\,^{\circ}\mathrm{C}^{-1}$

Table 2. Operating conditions for air cooled synchronous generator model.

Quantity	Symbol	Value
Initial value, rotor temperature	$T_\mathrm{r}\,(t=0)$	28 °C
Initial value, stator copper temperature	$T_\mathrm{s}\,(t=0)$	28 °C
Initial value, stator iron temperature	$T_\mathrm{Fe}\,(t=0)$	28 °C
Influent water temperature	T_w^c	3.8 °C
Water mass flow rate	$\dot{m}_\mathrm{w}$	53.9 kg/s
Air mass flow rate	$\dot{m}_\mathrm{a}$	49.2 kg/s
Rated rotor field current	I_f	1055 A
Rated stator terminal current, rated	I_t	5360 A
Stator iron generated heat	$\dot{Q}_\mathrm{Fe}^\sigma$	212 kW
Friction work	$\dot{W}_\mathrm{f}$	528 kW
Friction heating	$\dot{Q}_\mathrm{f}^\sigma$	$0.8\cdot\dot{W}_\mathrm{f}$

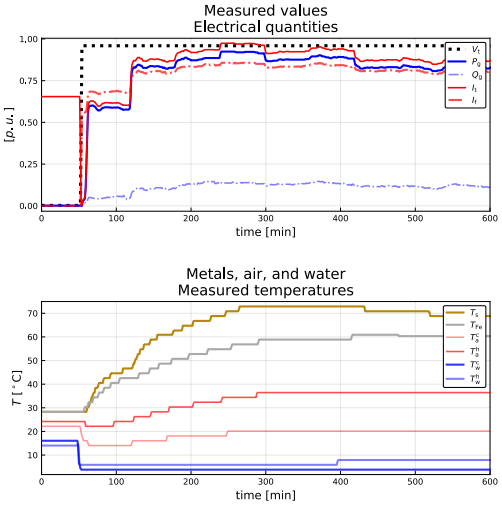

Figure 3. Experimental data for generator model from a 600 min heat-run test.

Table 3. Measured quantities.

Quantity	Symbol	Units	Sensor	#
Generator terminal voltage	V_t	kV	–	–
Active power of generator	P_g	MW	–	–
Reactive power of generator	Q_g	MVar	–	–
Rotor field current	I_f	A	–	–
Temperature of stator copper	T_s	°C	PT100	15
Temperature of stator iron	T_Fe	°C	PT100	4
Hot air temperature	T_a^h	°C	PT100 /CTD	2/2
Cold air temperature	T_a^c	°C	PT100 /CTD	2/2
Cold water temperature	T_w^c	°C	Analog	–
Hot water temperature	T_w^h	°C	Analog	–
Terminal current	$I_\mathrm{t}=\frac{P_g^2+Q_g^2}{\sqrt{3}\cdot V_\mathrm{t}}$	A	–	–

Table 4. Notations for the UKF and EnKF algorithms.

Symbol	Description
$x,\bar{x},\hat{x}$	State vector, its mean, its estimate
x_k	Vector x at time instance k
$\hat{x}_{k\|k-1}$	*a priori* estimate of x_k based on measurements up to time t_{k-1}
$\hat{x}_{k\|k}$	*a posteriori* estimate of x_k based on measurements up to time t_k
X	State co-variance
w	Process noise
v	Measurement noise
$\mathscr{W}$	Process noise co-variance
$\mathscr{V}$	Measurement noise co-variance
K	Kalman gain
$\mathscr{E}$	Innovation co-variance
Z	Cross co-variance
ε	Error between measurement and estimate

Table 5. Algorithm: UKF.

Initialization, $k = 1$:

$\hat{x}_{1|1} = \mathbb{E}(x_1) = \bar{x}_1$

$X_{1|1} = X_1$

for $k = 2,\ 3, ...$

Propagation step:

1. Generate *sigma points* using *unscented transformation*

$x^{(i)}_{k-1|k-1} = \hat{x}_{k-1|k-1} + \tilde{x}^{(i)}, \quad i \in \{1,2,...2n\}$

where, with Cholesky root R: $R^T R = n \cdot X_{k-1|k-1}$,

$\tilde{x}^{(i)} = R_{:,i}, \quad i \in \{1,2,...n\}$

$\tilde{x}^{(n+i)} = -R_{:,i}, \quad i \in \{1,2,...n\}$

2. Propagate sigma points through process model

$x^{(i)}_{k|k-1} = f\left(x^{(i)}_{k-1|k-1}, u_{k-1}, \bar{w}_k\right), \quad i \in \{1,2,...2n\}$

3. *a priori* state and co-variance estimate

$\hat{x}_{k|k-1} = \frac{1}{2n}\sum_{i=1}^{2n} x^{(i)}_{k|k-1}$

$X_{k|k-1} =$

$\frac{1}{2n}\sum_{i=1}^{2n}\left(x^{(i)}_{k|k-1} - \hat{x}_{k|k-1}\right)\left(x^{(i)}_{k|k-1} - \hat{x}_{k|k-1}\right)^T + \mathscr{W}_k$

Information update:

1. Propagate sigma points through measurement equation

$y^{(i)}_{k|k-1} = h\left(x^{(i)}_{k-1|k-1}, u_{k-1}, \bar{v}_k\right), \quad i \in \{1,2,...2n\}$

2. Predicted measurements

$\hat{y}_{k|k-1} = \frac{1}{2n}\sum_{i=1}^{2n} y^{(i)}_{k|k-1}$

3. Innovation and cross co-variance

$\mathscr{E}_{k|k-1} =$

$\frac{1}{2n}\sum_{i=1}^{2n}\left(y^{(i)}_{k|k-1} - \hat{y}_{k|k-1}\right)\left(y^{(i)}_{k|k-1} - \hat{y}_{k|k-1}\right)^T + \mathscr{V}_k$

$Z_{k|k-1} = \frac{1}{2n}\sum_{i=1}^{2n}\left(x^{(i)}_{k|k-1} - \hat{x}_{k|k-1}\right)\left(y^{(i)}_{k|k-1} - \hat{y}_{k|k-1}\right)^T$

4. Kalman gain

$K_k = Z_{k|k-1}\mathscr{E}^{-1}_{k|k-1}$

5. *a posteriori* update

$\varepsilon_{k|k-1} = y_k - \hat{y}_{k|k-1}$

$\hat{x}_{k|k} = \hat{x}_{k|k-1} + K_k\varepsilon_{k|k-1}$

$X_{k|k} = X_{k|k-1} - K_k\mathscr{E}_{k|k-1}K_k^T$

Table 6. Algorithm: EnKF

Initialization, $k = 1$:

$x^i_{1|1} \sim \mathscr{N}(\bar{x}_1, X_1),\ i \in \{1,2,...,n_p\}$

$w^i_k \sim \mathscr{N}(\bar{w}_1, \mathscr{W}_k),\ i \in \{1,2,...,n_p\}$

$v^i_k \sim \mathscr{N}(\bar{v}_1, \mathscr{V}_k),\ i \in \{1,2,...,n_p\}$

$\hat{x}_{1|1} = \frac{1}{n_p}\sum_{i=1}^{n_p} x^{(i)}_{1|1}$

$X_{1|1} = \frac{1}{n_p-1}\sum_{i=1}^{n_p}\left(x^{(i)}_{1|1} - \hat{x}_{1|1}\right)\left(x^{(i)}_{1|1} - \hat{x}_{1|1}\right)^T$

for $k = 2,\ 3, ...$

Propagation step:

1. Propagate particles through process model

$x^{(i)}_{k|k-1} = f\left(x^{(i)}_{k-1|k-1}, u_{k-1}, w^{(i)}_{k-1}\right)\ i \in \{1,2,...,n_p\}$

2. *a priori* state and co-variance estimates

$\hat{x}_{k|k-1} = \frac{1}{n_p}\sum_{i=1}^{n_p} x^{(i)}_{k|k-1}$

$X_{k|k-1} =$

$\frac{1}{n_p-1}\sum_{i=1}^{n_p}\left(x^{(i)}_{k|k-1} - \hat{x}_{k|k-1}\right)\left(x^{(i)}_{k|k-1} - \hat{x}_{k|k-1}\right)^T$

Information update:

1. Propagate particles through measurement equation

$y^{(i)}_{k|k-1} = h\left(x^{(i)}_{k-1|k-1}, u_{k-1}, v^{(i)}_{k-1}\right)\ i \in \{1,2,...,n_p\}$

2. Predicted measurements

$\hat{y}_{k|k-1} = \frac{1}{n_p-1}\sum_{i=1}^{n_p} y^{(i)}_{k|k-1}$

3. Innovation and cross co-variance

$\mathscr{E}_{k|k-1} =$

$\frac{1}{n_p-1}\sum_{i=1}^{n_p}\left(y^{(i)}_{k|k-1} - \hat{y}_{k|k-1}\right)\left(y^{(i)}_{k|k-1} - \hat{y}_{k|k-1}\right)^T$

$Z_{k|k-1} =$

$\frac{1}{n_p-1}\sum_{i=1}^{n_p}\left(x^{(i)}_{k|k-1} - \hat{x}_{k|k-1}\right)\left(y^{(i)}_{k|k-1} - \hat{y}_{k|k-1}\right)^T$

4. Kalman gain

$K_k = Z_{k|k-1}\mathscr{E}^{-1}_{k|k-1}$

5. *a posteriori* update of state and co-variance

$\varepsilon^{(i)}_{k|k-1} = y_k - y^{(i)}_{k|k-1}$

$x^{(i)}_{k|k} = x^{(i)}_{k|k-1} + K_k\varepsilon^{(i)}_{k|k-1}$

$\hat{x}_{k|k} = \frac{1}{n_p-1}\sum_{i=1}^{n_p} x^{(i)}_{k|k}$

$X_{k|k} = \frac{1}{n_p-1}\sum_{i=1}^{n_p}\left(x^{(i)}_{k|k} - \hat{x}_{k|k}\right)\left(x^{(i)}_{k|k} - \hat{x}_{k|k}\right)^T$

The UKF and EnKF are initialized with $\mathscr{W} = \text{diag}(4,4,4)$, $\mathscr{V} = \text{diag}(1,1)$ and $X = 10 \cdot \mathscr{W}$. Both the process noise w and measurement noise v are considered to be *white Gaussian noise* with zero-mean. The simulation time step Δt is set to 1 min and the total time of simulation is 584 min.

The simulation environment is the Julia programming language[2]. UKF and EnKF are compared based on root mean square error (RMSE) of innovation residuals, $\varepsilon = y_k - \hat{y}_{k|k-1}$, and computational speed[3].

4 Results and Discussion

The result for air and metals temperature estimation for Model 1 ($\hat{c}_p$, R) using UKF and EnKF for different particles is given in Figure 4.

Similarly, for four different models the estimates using UKF is given in Figure 5 and using EnKF with n_p=1000 is given in Figure 6.

The rotor copper temperature and air gap temperature estimates using EnKF, for Model 1, with different particles is given in Figure 7.

Figure 5 and 6 show a substantial difference in rotor copper and air gap temperature estimates for Model 3 and Model 4: models with temperature dependence in $\hat{c}_p$ tend to decrease the temperature of metals, but increase the air temperatures. In opposition to this, models with temperature dependence in R show an increase in both metal and air temperatures.

Figure 7 shows a comparison of EnKF depending on particle number n_p: with increased n_p, the estimates converge better and give a result similar to that of the UKF.

A comparison of UKF and EnKF with different number of particles, based on RMSE of innovation residuals and computational speed, is given in Table 7.

The results show that the RMSE of the UKF is larger than that of the EnKF. Furthermore, for EnKF the residuals decrease with increased number of particles n_p. The RMSE of residuals were lowest for Model 2 as compared to the other models. The computational time increases from UKF to EnKF and with n_p. The computational time also increases when the model complexity increases from Model 1 to 2 to 3 to 4 for EnKF with $n_p = 1000$.

5 Conclusions and future work

State estimation using UKF, and EnKF with different number of particles, have been studied for four different models. Results indicate that temperature dependent heat capacities increase air temperatures and reduce metal temperatures, while temperature dependent resistances increase all temperatures. EnKF shows better estimation accuracy than UKF, but with a penalty in computational speed. In the comparison, we have re-used the constant

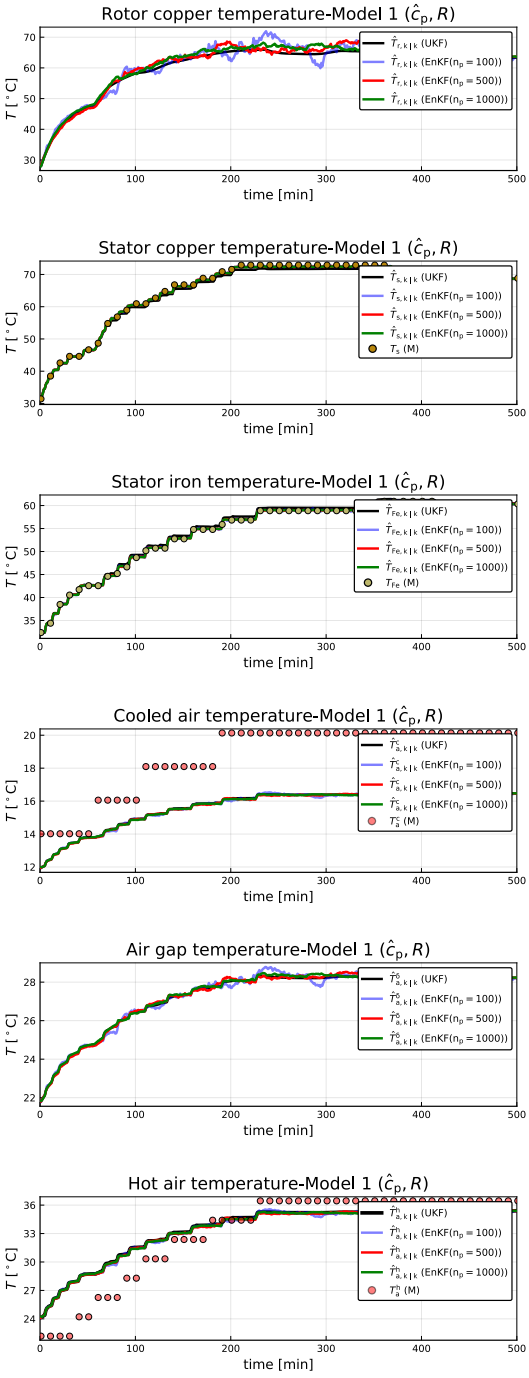

Figure 4. Air and metal temperature estimates using UKF and EnKF for Model 1 ($\hat{c}_p$, R). Subscript $k \mid k$ represents *a posteriori* estimate.

[2]Version 1.0.3 (2018-12-18)

[3]Processor: Intel(R) Core(TM) i7-7500U CPU @ 2.70GHz, 2901 Mhz, 2 Core(s), 4 Logical Processor(s)

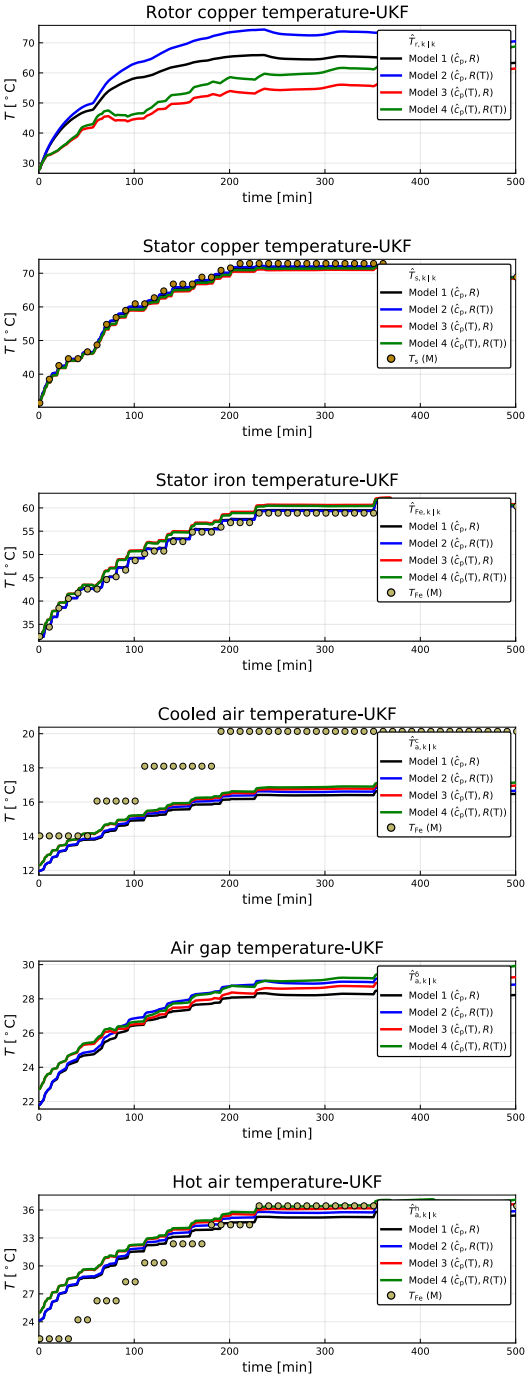

Figure 5. Air and metal temperature estimates using UKF for different models.

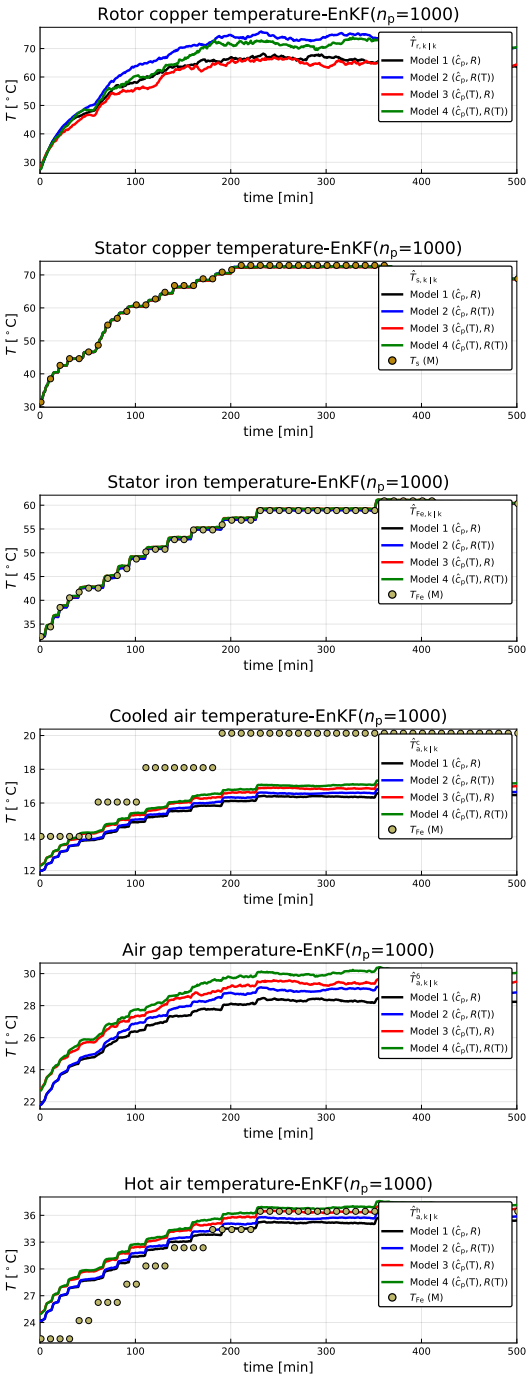

Figure 6. Air and metal temperature estimates using EnKF ($n_p = 1000$) for different models.

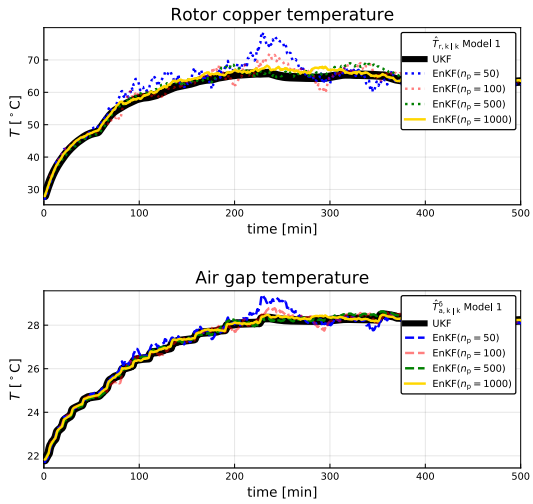

Figure 7. Rotor copper temperature and air gap temperature estimates using different number of particles for EnKF.

Table 7. Comparing Kalman filters with different models.

Model	KF	RMSE(ε)	Elapsed[s]
1	UKF	2.215	0.338
	EnKF($n_p = 50$)	2.066	1.088
	EnKF($n_p = 100$)	2.039	2.211
	EnKF($n_p = 500$)	2.010	10.860
	EnKF($n_p = 1000$)	2.012	26.343
2	UKF	1.652	0.744
	EnKF($n_p = 50$)	1.573	1.774
	EnKF($n_p = 100$)	1.524	3.414
	EnKF($n_p = 500$)	1.500	16.729
	EnKF($n_p = 1000$)	1.492	32.225
3	UKF	3.137	1.041
	EnKF($n_p = 50$)	2.735	3.238
	EnKF($n_p = 100$)	2.729	7.643
	EnKF($n_p = 500$)	2.705	36.663
	EnKF($n_p = 1000$)	2.701	58.595
4	UKF	2.730	0.798
	EnKF($n_p = 50$)	2.407	3.154
	EnKF($n_p = 100$)	2.342	5.287
	EnKF($n_p = 500$)	2.331	35.877
	EnKF($n_p = 1000$)	2.327	60.993

model parameters in all the models. Because these parameters essentially have been tuned for Model 1, it is difficult to draw strong conclusions on which model is best at this moment.

Future work will involve studies of (i) temperature dependent specific heat capacity for air and water with numeric solution of the resulting two point boundary value problem, (ii) extending the number of outputs from two (T_s, T_{Fe}) to four (T_s, T_{Fe}, T_a^c, and T_a^h), (iii) and a more formal model fitting for the various models.

References

Ole Magnus Brastein, Bernt Lie, Roshan Sharma, and Nils-Olav Skeie. Parameter estimation for externally simulated thermal network models. *Energy and Buildings*, 191:200–210, 2019. doi:10.1016/j.enbuild.2019.03.018.

ENTSO-E. Commission regulation (eu) 2016/631 of 14 april 2016 establishing a network code on requirements for grid connection of generators. Technical report, European Network of Transmission System Operators for Electricity, ENTSO-E Avenue de Cortenbergh 100 1000 Brussels Belgium, 2016.

Philip A. Hargreaves, B.C. Mecrow, and Ross Hall. Calculation of Iron Loss in Electrical Generators Using Finite-Element Analysis. *Industry Applications, IEEE Transactions on*, 48(5):1368–1373, May 2011. doi:10.1109/IEMDC.2011.5994805.

Bernt Lie. Solution, Project, FM1015 Modelling of Dynamic Systems. University of South-Eastern Norway, November 2018.

Bonnie J McBride, Michael J Zehe, and Sanford Gordon. Nasa glenn coefficients for calculating thermodynamic properties of individual species. Technical Report NASA/TP–2002-21155, NASA, NASA Center for Aerospace Information 7121 Standard Drive Hanover, MD 21076, 2002. URL `http://gltrs.grc.nasa.gov/GLTRS`.

Thomas Øyvang. *Enhanced power capability of generator unites for increased operational security*. PhD thesis, University of South-Eastern Norway, Faculty of Technology, Natural Sciences and Maritime Sciences University of South-Eastern Norway N-2018 Porsgrunn Norway, December 2018. ISBN: 978-82-7206-503-3 (print) ISBN: 978-82-7206-504-0 (online).

Dan Simon. *Optimal State Estimation: Kalman, H Infinity, and Nonlinear Approaches*. Wiley-Interscience, Hoboken, New Jersey, 2006.

Statnett. Fiks funksjonskrav i kraftsystemet [functional requirements in the power system]. Technical report, Statnett, 2012.

Michael J. Zehe, Sanford Gordon, and Bonnie J. McBride. CAP: A Computer Code for Generating Tabular Thermodynamic Functions from NASA Lewis Coefficients. Technical Report NASA/TP–2001-210959/REV1, NASA, NASA Center for Aerospace Information 7121 Standard Drive Hanover, MD 21076, 2002. URL `http://gltrs.grc.nasa.gov/GLTRS`.